Research Square

Preprints are preliminary reports that have not undergone peer review.
They should not be considered conclusive, used to inform clinical practice,
or referenced by the media as validated information.

A Lacticaseibacillus paracasei postbiotic rescues glucose-impaired serotonergic signalling in C. elegans and is antagonised by unmetabolised folic acid

Peter Onyango Ouma

peter.ouma.297@gmail.com

Sardar Patel University

Vasudev Thakkar

Sardar Patel University

Ankita Rathod

Sardar Patel University

Rutvi Faldu

Sardar Patel University

Harsh Joshi

Sardar Patel University

Paresh Chudasama

Sardar Patel University

Punam Bhende

Bhaikaka University

Rohan P. Modi

Pramukhswami Medical College, Bhaikaka University

Somashekhar Nimbalkar

Pramukhswami Medical College, Bhaikaka University

Research Article

Keywords: postbiotic, unmetabolised folic acid, Lacticaseibacillus paracasei, 10-formyl-tetrahydrofolate, folate receptor FOLR1, serotonergic neurons, calcium signaling, glucose stress, Caenorhabditis elegans

Posted Date: July 31st, 2026

DOI: https://doi.org/10.21203/rs.3.rs-10304798/v1

License: This work is licensed under a Creative Commons Attribution 4.0 International License.
Read Full License

Additional Declarations: No competing interests reported.

Abstract

Folic acid fortification has reduced birth defects worldwide, but in populations with high blood glucose or low vitamin B12 it has been linked to worse metabolic and neurological outcomes. Here we show, in *Caenorhabditis elegans*, that dietary excess glucose blunts the activity of serotonergic neurons and that a *Lacticaseibacillus paracasei* strain *AV47* restores it. A cell-free lysate (CFL) of the same organism, a postbiotic, reproduces the effect, which localises the activity to a soluble fraction. The defined one-carbon cofactor 10-formyl-tetrahydrofolate reproduces the rescue, whereas the synthetic vitamer unmetabolised folic acid (UMFA) blocks it specifically under glucose stress. This conditional, combined glucose-UMFA antagonism is the central mechanistic finding, and is consistent with competition for folate receptors. The postbiotic also preserved NSM neurite length, reduced intrauterine hatching while acutely stimulating egg-laying, shifted intestinal carbon flux from storage towards utilisation, and conferred an approximately seven-fold survival advantage under acute peroxide stress together with increased locomotion. We interpret these broader outcomes as the same diet effect propagating to downstream physiology rather than as independent mechanisms. Our results describe a defined microbial cofactor activity that opposes folate-aggravated glucose toxicity in this model, and suggest that 10-formyl-tetrahydrofolate is a plausible microbe deliverable effector worth testing in mammalian systems.

Introduction

Folic acid fortification has been a public-health success in reducing neural-tube defects, but its consequences in populations that are also burdened by hyperglycaemia or vitamin B12 insufficiency are less clear. When the dose of folic acid exceeds the conversion capacity of intestinal and hepatic dihydrofolate reductase, the unreduced vitamer, unmetabolised folic acid (UMFA), appears in the circulation. UMFA is now detected in nearly all serum samples from the US adult population, with concentrations above 1 nmol/L in roughly a third of adults (1). The convergence of dysglycaemia and excess folate has measurable consequences. In a 19-year follow-up of more than 15,000 NHANES adults, diabetic adults in the highest red-blood-cell folate quartile had higher all-cause and ischaemic-heart-disease mortality than those in the lowest at hazard ratio of 1.30, a relationship that was absent in non-diabetic adults (2). A meta-analysis of 16 studies in type 2 diabetic patients reported that vitamin B12 was significantly lower in patients with diabetic peripheral neuropathy than in diabetics without the complication (3). The molecular mechanism that connects this nutritional state to cellular dysfunction is not yet defined.

Caenorhabditis elegans offers an experimentally tractable system in which to study this convergence. The animal possesses a fully mapped 302-neuron nervous system in which serotonergic signaling is concentrated in the neurosecretory motor neurons (NSM) of the pharynx and the hermaphrodite-specific neurons (HSN) of the midbody (4). Calcium dynamics in these cells can be measured non-invasively with the genetically encoded indicator GCaMP (5), allowing direct measurement of the effect of glucose and folate species on neuronal function in real time. The worm reproduces several features of mammalian

glucose toxicity, including shortened lifespan, increased intestinal lipid storage and reduced neuronal output under chronic 2% dietary glucose (6). It also retains the major enzymes of the one-carbon cycle, which permits the study of folate and B-vitamin biology in a defined dietary background (7, 8).

A folate-receptor axis in *C. elegans* serotonergic neurons has recently been mapped. Peesapati and colleagues established that FOLR-1, an orthologue of human folate receptor alpha, gates the transient receptor potential melastatin channel GON-2 in a ligand-specific manner, with 10-formyl-tetrahydrofolate (10-formyl-THF) acting as the most potent agonist tested (9). The 10-formyl tetrahydrofolate is produced by some lactic acid bacteria in varying amounts and is structurally distinct from supplemental folic acid (10). A cross-species role for the same receptor in folate-responsive calcium signaling in mammalian neural progenitors has been reported (11), and the mammalian, crystallographic basis for 10-formyl-THF binding at folate receptor alpha has been described (12, 13).

Postbiotics are a tractable alternative to live probiotics. The International Scientific Association for Probiotics and Prebiotics (ISAPP) defines them as preparations of inanimate microorganisms or their components that confer a health benefit on the host, and a cell-free lysate (CFL) prepared by cell disruption, centrifugation, membrane filtration and spread-plate confirmation of the absence of viable cells falls within this definition (14). Lipoteichoic acid from heat-killed *L. paracasei* has been reported to engage TLR-2 signaling and to ameliorate ageing-related leaky gut and cognitive decline in mice (15), and live *L. paracasei* extends *C. elegans* lifespan in a DAF-16-dependent manner (16, 17). *L. paracasei* subsp. *tolerans* is a known producer of folate species, methylcobalamin, riboflavin and thiamine, whereas *L. delbrueckii* subsp. *bulgaricus* is relatively auxotrophic and produces predominantly other pteroates at lower amounts (18, 19). The two species therefore make a natural pharmacological contrast at the level of secreted cofactors.

Aim

We find that excess dietary glucose suppresses calcium transients in NSM neurons. Three open questions follow from this background. First, can *L. paracasei* rescue folate and glucose sensitive serotonergic phenotypes in *C. elegans* and can a cell-free preparation of *L. paracasei AV47* substitute for the live organism in reducing toxicity. Second, does the protective activity track the secreted-cofactor profile of the producing organism, including its folate output, or does it require contributions from cell-wall elements or short-chain fatty acids. Third, do the effects extend beyond calcium signaling into the metabolic, redox and locomotor outputs. We address these questions in an ordered series of experiments. We first ask whether *L. paracasei AV47* and its CFL rescues glucose-suppressed NSM calcium transients and whether different forms of folate are the active components of the lysate. We then ask whether the rescue is paralleled by preservation of NSM neurite length, by reduction of intrauterine hatching and acute stimulation of HSN-driven egg-laying, by altered intestinal carbon flux, improved survival under acute oxidative challenge and during free locomotion. Throughout, *L. paracasei AV47* is benchmarked against *L. delbrueckii* subsp. *bulgaricus* and against the standard *E. coli* OP50 diet (20). The probiotic of *L. paracasei AV47* and its secreted postbiotic, rather than a purified reagent, acts as

a potent agonist for serotonergic calcium activity; and the neuronal calcium transients level event is accompanied by coherent organismal outcomes.

Results

L. paracasei AV47 cell-free lysate rescues glucose-suppressed NSM calcium transients, and the activity behaves as a labile reduced folate that is functionally reproduced by 10-formyl-THF.

We first asked whether the cell-free lysate of a salivary isolate, *Lacticaseibacillus paracasei* subsp. tolerans strain AV47 could rescue the calcium-signaling deficit that chronic dietary glucose produces in NSM serotonergic neurons. Chronic 2% dietary glucose suppressed NSM calcium responses in animals fed *E. coli* OP50, and both the live *L. paracasei AV47* and its CFL restored NSM activity to levels indistinguishable from normal-glucose controls, localising the rescue to a soluble, secreted fraction (Fig. 1C-1F; n = 30 worms per condition). Post stimulus response magnitude was calculated as difference of mean F/F0 before and after application of bacterial stimulus. Under excess glucose, the post-stimulus to pre-stimulus fluorescence change in OP50-fed animals was 0.100 ± 0.024 F/F0, versus 0.516 ± 0.086 in the matched normal-glucose control, and a similar suppression occurred on *L. delbrueckii* ATCC 7830 (0.369 ± 0.051 versus 0.744 ± 0.114). Worms fed live *L. paracasei AV47* under glucose stress retained responses of 0.808 ± 0.089, statistically indistinguishable from their own normal-glucose control (0.662 ± 0.113) and far larger than the OP50-plus-glucose response. The CFL gave the same direction and magnitude of effect as the live cells, with a glucose response change of 0.872 ± 0.108 that did not differ from the live-bacterium response. Across the diet screen, response magnitude differed strongly by condition overall (Kruskal-Wallis $H(15) = 247.3$, $p < 0.001$), with OP50 versus *L. paracasei AV47* under glucose Dunn $p < 0.001$ and live versus CFL under glucose Dunn $p = 0.96$ (Fig. 1D, 1E). These data localise the diet-dependent rescue of NSM calcium transients to a soluble, cell-free output of *L. paracasei AV47*, ruling out a requirement for the live organism in this readout.

We next asked whether UMFA would interfere with the rescue, on the rationale that its systemic accumulation is the clinically relevant correlate of folate excess in dysglycaemic populations (1). Co-addition of 100 μM UMFA suppressed the *L. paracasei AV47* rescue only when animals were simultaneously exposed to dietary glucose; UMFA alone, without glucose, was inert at this readout. This conditional, combined glucose-UMFA antagonism is the central mechanistic observation of the study. Under glucose plus UMFA, response magnitude fell from 0.808 ± 0.089 to 0.100 ± 0.022 in live *L. paracasei AV47*, and from 0.872 ± 0.108 to 0.134 ± 0.040 in CFL-treated worms. All four glucose-plus-UMFA conditions converged on the lowest response group (means 0.100 to 0.138, sharing a single compact-letter group, Fig. 1E). UMFA without glucose did not reduce *L. paracasei AV47* responses (0.625 ± 0.099 versus 0.662 ± 0.113). Both pairwise Dunn comparisons of *L. paracasei AV47* with versus without UMFA under glucose were $p < 0.001$; UMFA alone versus no addition on *L. paracasei AV47*, Dunn $p = 0.97$; all pairwise comparisons among the four glucose-plus-UMFA conditions, $p > 0.6$. The conditional appearance of antagonism only where glucose and UMFA coincide is most simply explained by competitive displacement of a bacterially derived folate at FOLR-1 whose effect becomes perceivable

once the methylation arm is constrained by hyperglycaemia induced reactive oxygen species. Glucose driven changes in receptor trafficking and UMFA-mediated effects on folate uptake remain possible additional contributors.

To narrow the chemical identity of the active component, we tested three matched CFL preparations under glucose: native CFL, native CFL aged for two weeks at 4°C in the dark, native CFL from bacteria grown in the presence of dihydropteroate synthase (DHPS) inhibitor 1 mM sulfamethoxazole, and 50 nM 10-formyl-THF (Fig. 1D, 1F; n = 30 per condition). The activity was abolished by ageing and by sulfamethoxazole pre-treatment of the producer, and a single defined molecule, 10-formyl-THF, reproduced the rescue with comparable magnitude and time course to native CFL. Two-week ageing reduced the response from 0.872 ± 0.108 to 0.202 ± 0.040 (Dunn $p < 0.001$), consistent with a labile active component under refrigerated storage. Sulfamethoxazole pre-treatment produced a comparable reduction (to 0.101 ± 0.023; Dunn $p < 0.001$), placing the active component downstream of bacterial DHPS, possibly within the reduced-folate branch. Pure 10-formyl-THF produced a response statistically indistinguishable from native CFL (0.631 ± 0.092 versus 0.872 ± 0.108; Dunn $p = 0.55$, sharing a compact-letter group), with no detectable difference in latency to peak (Dunn $p = 0.28$). The dose-direction logic of competitive antagonism at the ligand level was also satisfied: co-addition of 100 µM UMFA suppressed pure 10-formyl-THF responses by 52% (0.631 ± 0.092 to 0.306 ± 0.043; Dunn $p = 0.015$) and native CFL responses by 85% (0.872 ± 0.108 to 0.129 ± 0.025; Dunn $p < 0.001$), whereas applying UMFA to sulfamethoxazole-inactivated CFL produced no further change (0.119 ± 0.028 versus 0.101 ± 0.023; Dunn $p = 0.90$). Overall, preparations differed strongly (Kruskal-Wallis $H(7) = 127.6$, $p < 0.001$). Three orthogonal perturbations therefore each abolished the rescue and a single defined molecule reproduced it, placing the active species within the reduced-folate branch and identifying 10-formyl-THF as functionally sufficient.

To anchor the chemical assignment in producer-level biology, we measured folate, cobalamin and pyridoxal-5-phosphate in the two lactobacillus CFL preparations by microbiological assay (Fig. 1B). *L. paracasei AV47* CFL was enriched in all three cofactors relative to *L. delbrueckii* CFL, consistent with a producer carrying a complete reduced-folate biosynthetic pathway. *L. paracasei AV47* CFL contained 100 µg/L cobalamin, 1,523 µg/L vitamin B6 and 1,241 µg/L total folate, versus 4 µg/L, 100 µg/L and 133 µg/L respectively in *L. delbrueckii* CFL, corresponding to approximately 25-fold more methylcobalamin, 15.7-fold more vitamin B6 and 9.3-fold more folate in the *L. paracasei AV47* preparation. The microbiological folate assay reports total folate activity and does not discriminate among vitamers, so the assignment of 10-formyl-THF as the proximate active species above is pharmacological rather than chemical. Because *L. paracasei AV47* carries the complete reduced-folate biosynthetic pathway, and a fraction of its secreted folate is expected to be in reduced forms, including 10-formyl-THF (18, 21).

Thus, three independent perturbations, extract ageing, DHPS inhibition and substitution with *L. delbrueckii* CFL, each abolished the rescue, and all converged on a comparable final response magnitude, whereas a single defined molecule, 10-formyl-THF, reproduced it.

L. paracasei AV47 preserves NSM neurite length under glucose stress and delays the onset of glucose-driven neurite growth retardation

We next asked whether the calcium-signaling rescue was paralleled by preservation of NSM neuronal architecture, because chronic dietary glucose has been shown to induce neurite retraction in *C. elegans* serotonergic and dopaminergic neurons (6, 22, 23), and netrin/UNC-6 guidance cues are established determinants of *C. elegans* neurite formation (24) susceptible to high glucose level induced dysfunction (25). Early developmental high glucose exposure, before the L3 stage, was associated with substantial shortening of both NSM processes, and removal of excess glucose after L3 did not restore neurite length, indicating that the structural lesion is set during early larval development and is not erased by later dietary correction (Fig. 2A). Under continuous excess glucose (G), subventral process length averaged 38.9 ± 0.8 µm and dorsal process length 39.3 ± 0.5 µm, whereas animals never exposed to high glucose before L3 (NG) showed significantly greater lengths of 54.3 ± 1.5 µm and 47.6 ± 0.4 µm respectively, corresponding to an approximately 28% shorter subventral and 18% shorter dorsal process under early glucose (subventral, G vs NG, Wilcoxon $p = 5.8 \times 10^{-12}$; dorsal, G vs NG, $p = 1.0 \times 10^{-15}$). High glucose withdrawal at L3 (GtoNG) did not restore neurite architecture, with subventral and dorsal lengths remaining significantly reduced relative to NG animals (37.6 ± 0.9 µm, $p = 1.6 \times 10^{-12}$; and 40.7 ± 0.6 µm, $p = 2.9 \times 10^{-14}$ respectively). In contrast, delayed excess glucose introduction after L3 (NGtoG) did not reproduce this shortening: both processes remained far longer than in G or GtoNG animals (subventral 48.8 ± 1.2 µm; dorsal 50.8 ± 0.6 µm), and dorsal process length was in fact modestly but significantly greater than in NG animals (NG vs NGtoG, $p = 0.0012$), while the subventral process was slightly shorter than in NG yet still well above the early-glucose groups (NG vs NGtoG, $p = 0.00032$). This is consistent with post-L3 neurites being largely insensitive to excess glucose once the early developmental window has closed. NSM neurite shortening therefore behaves as a critical-period phenomenon, written during early larval development. NSM abnormality induced by high glucose early exposure have been reported in other studies to include NSM dorsal branch that is missing or have an abnormal length as it either did not reach the mid region of the isthmus or extended beyond (6).

To determine whether bacterial background or folate supplementation modified the structural lesion, we stratified the dataset according to pre-L3 glucose history (Fig. 2B, 2C). Among animals exposed to glucose before L3, *L. paracasei AV47* preserved NSM neurite length whereas exogenous folic acid did not, indicating that structural protection tracks bacterial diet rather than supplemental folate. Folic acid supplementation had no significant effect on either subventral or dorsal process length under glucose: subventral lengths were 39.2 ± 0.6 µm without folate and 37.3 ± 1.0 µm with 100 µM folic acid ($p = 0.11$), and dorsal lengths were 39.5 ± 0.5 µm and 40.5 ± 0.6 µm respectively ($p = 0.24$). By contrast, animals reared on *L. delbrueckii* had shorter subventral and dorsal processes (34.3 ± 0.5 µm and 37.1 ± 0.5 µm) than animals reared on *L. paracasei AV47* (42.3 ± 0.6 µm and 42.9 ± 0.2 µm), corresponding to approximately 24% greater subventral and 16% greater dorsal length on *L. paracasei AV47* (subventral $p = 1.2 \times 10^{-15}$; dorsal $p < 2.22 \times 10^{-16}$). Under equivalent developmental glucose exposure, then, *L. paracasei AV47* preserved NSM neuronal architecture whereas exogenous folic acid did not affect it significantly.

For completeness, we asked whether bacterial diet or folate supplementation altered neurite morphology in the absence of pre-L3 glucose. In animals not exposed to glucose before L3, neither manipulation significantly altered neurite length, indicating that the structural protection by *L. paracasei AV47* is conditional on the glucose insult rather than a generic baseline lengthening effect. Subventral process lengths remained between approximately 49 and 53 μm and dorsal processes between approximately 49 and 51 μm across conditions, and no folate or bacterial comparison reached significance (folate: subventral $p = 0.63$, dorsal $p = 0.11$; organism: subventral $p = 0.056$, dorsal $p = 0.056$). Collectively, these findings indicate that the major driver of NSM neurite shortening is excess glucose exposure during early larval development, and that *L. paracasei AV47* provides substantial structural protection under these conditions, independently of exogenous folic acid.

L. paracasei AV47 CFL reduces intrauterine hatching and acutely stimulates HSN-driven egg-laying through a sulfamethoxazole-sensitive component

The calcium rescue and the neurite preservation were both measured in NSM neurons. We next asked whether the same bacterial intervention operates at the HSN-driven behavioural output of egg-laying, which is the canonical assay for HSN serotonergic competence (26, 27). When the egg-laying rate falls below the rate of embryo production, embryos are retained and hatch internally, a state termed intrauterine hatching (IUH), or bagging, that culminates in the death of the adult and the liberation of L1 larvae from within the cuticle (*28*; Fig. 3A). IUH is therefore a direct functional readout of HSN-NSM circuit competence under chronic dietary stress.

Under chronic 2% dietary glucose, all three lactobacillus-related interventions reduced IUH relative to OP50, with *L. paracasei AV47* CFL giving the lowest IUH burden; in the absence of glucose, IUH rates converged across diets, identifying glucose as the upstream determinant and bacterial diet as the modifier (Fig. 3B). Under chronic glucose, OP50-fed cohorts showed the highest IUH burden (63.14 ± 2.80% bagged hermaphrodites per cohort of 30), reduced to 44.57 ± 2.15% on live *L. paracasei AV47*, 47.43 ± 2.37% on *L. delbrueckii* and 36.29 ± 0.76% on *L. paracasei AV47* CFL. Under normal-glucose conditions, IUH rates converged across all dietary groups (range 18.17 to 21.00%) with no significant inter-strain differences. All glucose-condition pairwise comparisons were significant (Tukey HSD $p < 0.0001$). Glucose is therefore the upstream determinant of the IUH, and the bacterial diet modifies the magnitude of the response.

We then asked whether the developmental-timing dependence observed for NSM neurites also applied to IUH. The timing of glucose exposure was decisive for the magnitude of IUH, paralleling the NSM neurite data above; pre-L3 exposure was substantially more damaging than adult-only exposure, and *L. paracasei AV47* CFL reduced the burden across regimens. Animals raised on 2% glucose from hatching and transferred to glucose-free medium after the L3 moult (GlucoseToNoGlucose) retained IUH levels of 56.40 ± 5.99% on OP50, significantly different from, but only slightly below, the chronic-glucose phenotype at 63.14 ± 2.80% ($p = 0.025$). Conversely, animals raised without glucose and introduced to 2% glucose only after L3 (NoGlucoseToGlucose) showed IUH of 31.33 ± 3.74% on OP50, approximately 50%

lower than the chronic-glucose phenotype ($p < 0.001$). GlucoseToNoGlucose elicited significantly more IUH than NoGlucoseToGlucose ($p < 0.001$), indicating that developmental glucose exposure is more potent than adult-phase exposure in driving IUH. On *L. paracasei AV47* CFL, the IUH burden under GlucoseToNoGlucose fell to 33.07 ± 1.83%, a 23 percentage point reduction relative to OP50 in the same regime.

To distinguish the cumulative IUH phenotype from acute HSN motor competence, we measured the rate of egg release into buffer at 5, 10 and 60 min in wild-type day-1 adults exposed to *L. paracasei AV47* extract (Pextract), *L. delbrueckii* extract (Bextract) or sulfamethoxazole-pretreated *L. paracasei AV47* extract (SUX) (*26, 27*; Fig. 3C). *L. paracasei AV47* extract significantly increased acute egg-laying at all three time points, *L. delbrueckii* extract produced no significant change, and sulfamethoxazole pre-treatment of the producer abolished the stimulatory activity. Pextract increased egg-laying at 5 min ($p = 0.027$), 10 min ($p = 0.010$) and 60 min ($p = 0.012$). Bextract produced no significant change at any time point (all $p > 0.16$). Sulfamethoxazole pre-treatment of the producer abolished the stimulatory activity of the extract (all $p > 0.05$ after SUX). Two independent perturbations of the *L. paracasei AV47*-derived signal, sulfamethoxazole pre-treatment and substitution with *L. delbrueckii*, therefore each removed the egg-laying stimulation, the same pattern that we observed for the calcium rescue.

L. paracasei AV47 redirects intestinal carbon flux from lipid storage towards utilisation in a one-carbon-cycle-sensitive manner

The experiments above isolate a defined activity in directly serotonergic readouts. We next asked, as a set of secondary, consistency-checking outcomes, whether the same bacterial intervention propagates to intestinal carbon flux that is independently disturbed by glucose. Serotonergic output is one input among several into intestinal lipolysis through mod-1 and ser-7 signaling and the ATGL-1/KAT-1 lipolytic axis (29–31). We therefore measured two coupled readouts: residual culture-medium glucose, which falls as imported glucose is committed to oxidative metabolism, and intestinal neutral-lipid storage, visualised by Sudan III staining. Residual glucose was assayed across four bacterial diets (OP50, live *L. paracasei AV47*, *L. paracasei AV47* CFL and *L. delbrueckii*) and seven one-carbon-metabolism (OCM) perturbations: vehicle control; S-adenosyl-L-methionine (SAM, 50 µM); S-adenosyl-L-homocysteine (SAH, 50 µM); methotrexate (MTX, 1 µM); 100 µM UMFA; MTX plus SAM; and SAM plus UMFA ($n = 7$ replicates per group; Fig. 4A) with a starting glucose enrichment of 2000 mg/dL in S complete medium and 20 worms/µL and change recorded after 72 hours.

Under control conditions, *L. paracasei AV47* produced the lowest residual medium glucose of any diet, SAM supplementation reduced residual glucose across all bacterial conditions, and SAH elevated residual glucose most prominently on *L. delbrueckii* while leaving *L. paracasei AV47* and its CFL unchanged, indicating a postbiotic-conferred resilience to methyltransferase inhibition. Under control, *L. paracasei AV47* gave 1,767 ± 228 mg/dL residual glucose, lower than OP50 (2,225 ± 436 mg/dL). SAM supplementation reduced residual glucose by 40 to 55% across diets (OP50 971 ± 252; live *L. paracasei AV47* 886 ± 756; *L. paracasei AV47* CFL 921 ± 339; *L. delbrueckii* 1,347 ± 306 mg/dL; all $p \leq 0.05$ relative to

the cognate no-SAM control), in the direction expected if SAM-driven activation of AMPK/AAK-2 improves metabolic flux (32–34). SAH produced the largest elevations in residual glucose of any treatment, most prominently on *L. delbrueckii* (3,031 ± 541 mg/dL; $p < 0.0001$ relative to SAM), in the direction expected if methyltransferase inhibition impairs glucose utilisation. Importantly, SAH did not significantly elevate residual glucose on *L. paracasei AV47* ($p = 0.712$), and the *L. paracasei AV47* CFL reproduced this resilience. Methotrexate and UMFA both elevated residual glucose towards or above the 2,000 mg/dL starting concentration, consistent with restriction of one-carbon flux delaying glucose oxidation. One interpretation of the postbiotic resilience is that the secreted-cofactor pool of *L. paracasei AV47*, which includes methylcobalamin and pyridoxal-5-phosphate as measured above, buffers methyltransferase inhibition, although a contribution from other, non-cofactor components of the CFL is not excluded by these data. Because residual medium glucose reflects microbial as well as host metabolism, the values that rose above the 2,000 mg/dL starting concentration are most plausibly explained by the live bacteria liberating additional glucose from other constituents of the medium, something the cell-free lysate, which contains no viable cells, cannot do. This points to a possible practical advantage of a postbiotic over a live probiotic, in that it would not be expected to raise the glycemic index of food by augmenting the hosts digestive enzymes.

As a qualitative companion observation, Sudan III staining indicated reduced intestinal neutral-lipid accumulation on *L. paracasei AV47* CFL relative to OP50 and *L. delbrueckii*, in the direction expected if more imported glucose is committed to oxidative use and less remains for lipogenesis (Fig. 4B). In the OP50 and *L. delbrueckii* groups the worms displayed broadly stained intestines indicative of accumulated lipid stores, whereas on *L. paracasei AV47* CFL the intestines stained less intensely, consistent with reduced neutral-lipid accumulation. The direction of the observation agrees with the residual-glucose data, in that on *L. paracasei AV47* and its CFL more imported glucose appears committed to oxidative use and less remains for lipogenesis and droplet deposition. One possibility is diet-supported, NSM-driven ATGL-1/KAT-1 activation and triglyceride mobilisation, possibly combined with SAM-driven AMPK-mediated metabolic shift. Taken together, the residual-glucose and Sudan III observations point in the same direction across diets and cohere with the receptor-level rescue, the neurite preservation and the egg-laying rescue described above.

L. paracasei AV47 CFL increases survival under acute oxidative stress and raises locomotor output

If the bacterial intervention acts in part by supplying cofactors that feed the glutathione and methylation pools, the same diets should produce directionally similar effects on stress-resilience phenotypes. As a further consistency check, we tested acute peroxide survival and body bending in matched cohorts fed OP50, live *L. paracasei AV47*, *L. paracasei AV47* CFL or *L. delbrueckii*, comparing the live and CFL preparations deliberately to separate secreted-component activity from any effect requiring ongoing bacterial metabolism.

L. paracasei AV47 CFL and the live organism each conferred an approximately seven-fold survival advantage over OP50 after 6 h of acute 2 mM hydrogen peroxide exposure, with no significant difference

between live and CFL preparations at late time points, indicating that the protection is mediated by stable secreted components rather than by ongoing bacterial metabolism (Fig. 5A; n = 18 wells of 10 animals per condition, three replicate plates). Baseline survival did not differ between groups (Tukey $p > 0.09$). Divergence emerged by 1 h: live *L. paracasei AV47* (97.2 ± 1.7%) and *L. paracasei AV47* CFL (99.1 ± 1.9%) both outperformed OP50 (88.5 ± 4.3%; $p = 0.002$ and $p < 0.001$ respectively), with the two *L. paracasei AV47* conditions not differing ($p = 0.715$). By 4 h a three-way separation was evident (OP50 25.8 ± 4.9%, *L. paracasei AV47* CFL 50.8 ± 4.2%, live *L. paracasei AV47* 63.1 ± 5.8%; all pairwise $p < 0.001$). By 6 h, OP50 survival had fallen to 4.5 ± 2.4%, while live *L. paracasei AV47* and *L. paracasei AV47* CFL sustained 31.8 ± 5.5% and 35.3 ± 4.6% respectively, an approximately seven-fold survival advantage for both supplemented conditions over OP50 (both $p < 0.001$). Two-way ANOVA returned significant main effects of strain ($p < 0.001$) and time ($p < 0.001$), and a significant strain-by-time interaction ($p < 0.001$). Live and CFL preparations did not differ significantly at 5 or 6 h ($p = 0.169$ and 0.330). This late-stage convergence indicates that the bulk of the protection is mediated by stable, secreted components of the CFL rather than by metabolic activity of the live organism.

As a parallel behavioural integration of serotonergic, mitochondrial and neuromuscular function, we then measured complete sinusoidal body bends per minute in buffer (*35*; Fig. 5B). Live *L. paracasei AV47* and *L. paracasei AV47* CFL each approximately doubled body-bending output relative to OP50, with no significant difference between the live and CFL preparations, again localising the activity to a secreted component. OP50-fed animals performed 22.5 ± 12.0 bends/min, compared with 50.9 ± 16.6 bends/min on live *L. paracasei AV47* ($\Delta = +28.5$; 95% CI 17.2 to 39.7; $p < 0.001$) and 50.0 ± 15.4 bends/min on *L. paracasei AV47* CFL ($\Delta = +27.5$; 95% CI 16.3 to 38.8; $p < 0.001$), an approximately 125% increase relative to OP50. Live and CFL preparations did not differ ($\Delta = 0.95$; $p = 0.978$). One-way ANOVA returned a significant effect of dietary condition ($p < 0.001$, $\eta^2 = 0.46$), with strain accounting for 46% of total locomotor variance. As in the peroxide assay, the live-and-CFL equivalence indicates that the activity is carried by stable secreted components of the lysate rather than by ongoing bacterial metabolism.

Across both late-phase readouts the CFL matched the live bacterium, and both exceeded OP50 by directionally consistent margins, completing the pattern in which the secreted activity tracks every phenotype examined.

Discussion

We show that a change of bacterial diet from *E. coli* OP50 to a cell-free lysate of *L. paracaseiAV47*, was sufficient to protect *C. elegans* against a coordinated set of phenotypes elicited by combined dietary glucose and folic acid stress. This rescue sits within a now established *C. elegans* glucose toxicity phenotype space, in which dietary glucose shortens lifespan and downregulates DAF16/FOXO (36), drives advanced glycation and reactive oxygen species lesions that mirror mammalian diabetic damage (23), attenuates dopaminergic function (22), and produces morphology and reproductive defects in serotonergic neurons (6). Live *L. paracasei AV47* has previously been shown to extend *C. elegans* lifespan through DAF16-dependent mechanisms (16, 17), establishing the biological plausibility of its protective

effect. The decisive pharmacology is convergent. Three orthogonal manipulations, including two-week ageing of the lysate, growth of the producer in the DHPS inhibitor sulfamethoxazole, and substitution with *L. delbrueckii*, each abolished the calcium transients rescue, whereas a single defined molecule, 10-formyl-tetrahydrofolate, reproduced it. The simplest compatible explanation with the observations is that the active factor is a labile DHPS-derived reduced folate, for which 10-formyl-THF is functionally sufficient. The 10-formyl-THF is the same vitamer that Peesapati and colleagues identified as the most potent FOLR-1 agonist in *C. elegans* serotonergic neurons, and our data are pharmacologically consistent with engagement of that axis with increase in egg laying response occurring similarly and quickly within 5 minutes. Our advance over that work is: the activity is delivered by a secreted postbiotic rather than a purified reagent and is antagonised by the synthetic vitamer UMFA only under combined glucose stress; the axons of the same neurons become shortened under excess glucose stress in a developmental critical-period (before L3).

Unmetabolised folic acid suppressed the rescue only when animals were simultaneously glucose overloaded, and adding UMFA to sulfamethoxazole inactivated lysate produced no further effect (Fig. 1D). A competitive-ligand model account for this economically as both UMFA and 10-formyl-THF bind FOLR1 but only 10-formyl-THF is able to induce the conformational change that opens the calcium channel GON2 to affect serotoninergic tone(9). Chronic hyperglycaemia drives mitochondrial overproduction of superoxide, the unifying lesion behind diabetic tissue damage in mammals (37, 38) and a documented consequence of high glucose in *C. elegans* (23). The reduced folate methylation arm is conspicuously redox sensitive at the very step that regenerates methyl groups: cobalamin dependent methionine synthase proceeds through a supernucleophilic cob(I)alamin intermediate that is intermittently oxidised to inactive cob(II)alamin and must be salvaged by S-adenosylmethionine-dependent reductive reactivation (39). Under a sustained superoxide load this reactivation cycle is expected to lag, which narrows the kinetic margin by which a bacterial reduced folate out-competes UMFA. In the absence of that oxidative pressure the endogenous ligand prevails and UMFA is not as inhibitory, exactly as we observed. The model is intriguing because it is conditional in the same way that the data are, and it predicts antagonism only where glucose and UMFA coincide, but it is not the only candidate. Excess glucose driven changes in folate receptor trafficking, for which the human receptor offers structural precedent in adopting distinct trafficking-competent conformations (13), altered intracellular folate handling, or direct perturbation of the neuronal methionine cycle which is itself a determinant of diet-dependent behavior in *C. elegans* serotonergic neurons (8), could each play a part in reproducing the pattern.

The neurite data add a developmental dimension that sharpens the translational reading. NSM process shortening was governed by excess glucose presence before the L3 stage: pre-L3 exposure shortened the subventral process by roughly 28% and the dorsal process by roughly 18%, withdrawal of glucose after L3 failed to restore them, and introduction of glucose only after L3 left neurite architecture essentially intact, with both processes remaining far longer than under early glucose exposure (Fig. 2A). The structural lesion therefore behaves as a critical-period phenomenon, written during early larval development and not erased by later dietary correction. Against this fixed structural background, *L.*

paracasei AV47 preserved neurite length under the same developmental excess glucose exposure, and did so independently of supplemental folic acid. Glucose imposes a partly irreversible axonal structural cost during a developmental window, yet the egg-laying circuit shows partial functional recovery due to the lysate. A critical-period sensitivity of folate-dependent neurodevelopment is not without precedent, as folate-receptor signaling is required during mammalian neural-tube formation (11), and early-life folate/B12 imbalance carries lasting metabolic consequences in human cohorts (40). Our data place a tractable developmental window around the phenomenon in a genetically accessible model.

The *L. paracasei* AV47 lysate altered several distinct phenotypes at once, most of which are known to be influenced by serotonergic tone. We are explicit that calcium signaling, neurite architecture, egg-laying, intestinal lipid handling, oxidative-stress survival and locomotion are governed by distinct genetic circuits: serotonergic lipolysis through mod-1 and ser-7 (29, 30), the SKN-1/glutathione axis for peroxide defense (41), and the integrated serotonergic, mitochondrial and neuromuscular control of locomotion (35). The parallel direction of effect therefore cannot be ascribed to a single regulatory node in the animal but the node can play a detectable part. Our interpretation is that the lysate supplies a pool of cofactors, each feeding more than one circuit. The vitamer profiling makes this concrete: *L. paracasei AV47* lysate carried roughly 100-fold more cobalamin and around an order of magnitude more folate and vitamin B6 than the comparator diets. Cobalamin sustains the very methionine-synthase reaction that hyperglycemic superoxide threatens (39); pyridoxal-5-phosphate is the shared cofactor of serotonin biosynthesis and of the transsulfuration enzymes that convert homocysteine to cysteine and onward to glutathione (42), a route that supplies roughly half of the cellular glutathione pool and is itself up-regulated under oxidative stress (43); and 10-formyl-THF engages the FOLR-1/GON-2 axis. This transsulfuration link is particularly satisfying, because it threads the same one-carbon machinery implicated in the calcium rescue through to the glutathione pool that sets peroxide survival, offering a coherent connection between the neuronal and the redox phenotypes. The metabolic readout fits the same logic: the fall in residual medium glucose was amplified by S-adenosylmethionine and lies in the direction expected if SAM-driven activation of AMPK/AAK-2 enhances oxidative flux (32, 33). Which of these inputs is rate-limiting for any single phenotype is the obvious next question. Body bending in *L. paracasei AV47* diet, was higher than OP50 diet. As muscle is the principal organismal sink for circulating glucose, and the spontaneous locomotion that the body-bending assay measures integrates serotonergic modulation, mitochondrial ATP supply and neuromuscular junction integrity into a single readout (35). The clinical analogue is informative: people with sustained dysglycaemia move less and tire faster, a phenotype attributed by the superoxide model to the same mitochondrial source as the tissue damage of diabetic complications (37, 38). Because failure of HSN-driven egg-laying is a cumulative consequence of disrupted serotonergic competence in this animal, we expected, and observed, parallel improvements at this behavioural output. Intrauterine hatching is the canonical phenotype that follows when egg release falls below embryo production (28), and hyperglycaemia is its principal upstream determinant in our data, attenuating serotonergic signaling and disorganising the egg laying circuits (6, 36). *L. paracasei AV47* CFL produced the lowest intrauterine hatching under chronic hyper glucose; acute *L. paracasei AV47* extract elevated egg-laying at all measured time points,

consistent with the established HSN behavioural circuitry (26, 27); and sulfamethoxazole pre-treatment of the producer abolished the stimulation. The same two perturbations, aging and inhibition of DHPS, that removed the calcium rescue also removed the egg-laying stimulation, the simplest behavioural extension of a single receptor-level rescue. Because our design changes only the bacterial diet, the differences we observe are attributable to diet in this experimental setting. It is also important to acknowledge that *C. elegans* models remain inherently limited in their ability to fully recapitulate human neural architecture and therefore translation of these findings will require validation in more physiologically relevant systems.

These observations bear on a genuine and unresolved human puzzle. Folic acid fortification is among the most successful public-health measures of the past three decades, yet several large datasets describe a darker edge where folate excess meets dysglycaemia: higher all-cause and ischaemic mortality among diabetic adults in the highest red-blood-cell-folate quartile (2), rising gestational-diabetes prevalence in the period after mandatory fortification (44), and the high-folate, low-B12 phenotype that predicts insulin resistance in offspring (40). None of these signals has yielded a single agreed molecular mechanism. Our data suggest a candidate frame: that what matters may be less the quantity of folate than its chemical form, that is, reduced bacterial vitamers versus synthetic UMFA, read against a metabolic context in which hyperglycaemic oxidative stress has narrowed one-carbon flux. In that frame the synthetic vitamer becomes a liability precisely where the reduced vitamer is most needed.

Because the observed postbiotic activity can be attributed to a defined class of secreted metabolites, namely the reduced folates produced by *L. paracasei* AV47 it is, in principle, amenable to quantification, standardisation and controlled dosing. These characteristics may facilitate the development of reproducible postbiotic formulations. Furthermore, both *L. paracasei* AV47 and its cell-free lysate represent potential candidates for adjunctive intervention in conditions characterised by concurrent hyperglycaemia and elevated UMFA exposure. On validation in more physiologically relevant models, the present findings provide a foundation for exploring microbiome-derived folate metabolites as modulators of diet-induced neuronal dysfunction.

Methods

Worm strains and culture

Caenorhabditis elegans wild-type N2 Bristol and the NSM reporter strains used for imaging were maintained at 20°C on Nematode Growth Medium (NGM) seeded with Escherichia coli OP50 by standard procedures (20, 45). Two NSM-specific reporter strains were used. Strain ET566 (unc-119(ed3) III; ekIs27[pCFJ350/tph-1pDE::GCaMP7s::P2A::mScarlet::unc-54 3'UTR]) carries GCaMP7s together with mScarlet as a ratiometric reporter, with the P2A ribosome-skipping sequence ensuring co-expression of both fluorophores from a single transcript. Strain ET571 (lite-1(ce314) X; ekIs26[pCFJ350/tph-1pDE::GCaMP7b::unc-54 3'UTR] II) carries GCaMP7b alone and is not ratiometric. Its lite-1 background reduces the photophobic response to blue light, which allows animals to be imaged without the

excessive blue-light avoidance shown by lite-1(+) animals. For the ratiometric ET566 strain a high-quality green emission filter is used, because the brighter mScarlet signal can otherwise bleed through into the green GCaMP channel. ET571 (GCaMP7b) was used for calcium imaging (Fig. 1), and the mScarlet channel of ET566 was used for NSM neurite morphometry (Fig. 2). Age synchronisation was by alkaline hypochlorite treatment of gravid adults (46), and recovered embryos were grown to L4 or day-1 adulthood on the indicated bacterial diet. Glucose-loaded plates were prepared by adding D-glucose to autoclaved NGM after cooling to 55°C, to a final concentration of 2% (w/v), to avoid caramelisation. Folic acid (Sigma, F8758) was supplied at 100 µM where indicated.

Bacterial strains and cell-free lysate preparation

A salivary isolate of *Lacticaseibacillus paracasei* subsp. *tolerans strain AV47* was recovered from the saliva of a healthy, non-diabetic adult donor in Gujarat, India (August 2025) under institutional ethics approval number IEC/BU/2025/Ex.49/184/2025. The isolate was identified by 16S rRNA gene sequencing (Sanger dideoxy method); the 1,336-bp partial sequence is deposited in NCBI GenBank under accession PZ458082. A type strain of *Lactobacillus delbrueckii subsp. bulgaricus* and *Escherichia coli OP50* were obtained from the departmental culture collection. *Lactobacilli* were grown in de Man, Rogosa and Sharpe (MRS) broth at 37°C for 24 h to stationary phase, and OP50 was grown in LB at 37°C overnight. Cell-free lysates were prepared as follows. The bacterial culture was grown to the stationary phase and harvested by centrifugation at 6,000 × g for 10 min at 4°C. The cell pellet was washed twice with cold deionized water and resuspended to the desired cell density. The suspension was incubated with lysozyme (1 mg/mL) for 30 min at 37°C to weaken the cell wall, followed by 20 passes through a sterile 26-gauge needle to promote mechanical disruption. The suspension was then sonicated for 5 min in an ice bath to complete cell lysis while minimizing heat-induced degradation of labile intracellular metabolites. Following sonication, cell debris was removed by centrifugation at 4,000 × g for 10 min at 4°C, and the clarified lysate was passed through a 0.22 µm PVDF membrane filter to obtain a sterile cell-free intracellular extract. The absence of viable cells was confirmed by spread-plating an aliquot of the filtered lysate on MRS or LB agar and incubating for 48 h at 37°C, with no colony-forming units recovered; the resulting CFL is therefore a postbiotic preparation in the ISAPP-defined sense (14). Native CFL preparations were stored at 4°C in the dark and used within 1 h of preparation. Aged CFL was prepared by holding native CFL at 4°C for 14 days in the dark before use. Sulfamethoxazole-treated CFL was prepared by extraction from bacteria grown in 1 mM sulfamethoxazole at 37°C through the entire culture period. Pure 10-formyl-tetrahydrofolate was prepared as a 50 nM working solution and used within 1 h.

Microbiological vitamin assays

Folate was quantified by turbidimetric *Lactobacillus casei* ATCC 7469 assay, methylcobalamin by turbidimetric *Lactobacillus delbrueckii* ATCC 7830 assay, and pyridoxal-5-phosphate (vitamin B6) by *Saccharomyces cerevisiae* ATCC 9080 turbidimetric assay (47, 48). Three biological replicates were

measured for each strain, with three technical replicates per biological replicate. Welch t-tests on log-transformed values were used for pairwise comparisons.

Calcium imaging and neurite morphometry

Day-1 adult ET571 (tph-1p::GCaMP7b) animals were transferred to OP50-free M9 buffer for 5 h to allow intestinal clearance, then immobilised on a 10% agarose pad with 1 mM levamisole on a 22 × 22 mm coverslip. Imaging used an epifluorescence microscope with a 63× oil-immersion objective, a GFP/FITC filter cube and an sCMOS camera at 4 Hz for 5 min per animal. Stimulus (bacterial diet, CFL or pure 10-formyl-THF, with or without 100 µM UMFA) was applied to the pad at t = 50 s. F/F0 was calculated for a manually defined NSM cell-body region of interest, with F0 the mean fluorescence over the first 40 s, and response magnitude was taken as the mean post-stimulus minus pre-stimulus F/F0 over the 250 s following the stimulus. n = 30 worms per condition were imaged across three independent days. For neurite morphometry, day-3 adult ET566 animals were imaged on the same configuration through a TRITC filter (mScarlet channel, calcium-independent). Subventral and dorsal NSM processes were traced manually in ImageJ by an observer blinded to dietary and glucose condition. Four glucose regimes were tested: continuous 2% glucose as high-glucose (G), normal-glucose (NG), high-glucose-to-normal-glucose at L3 (GtoNG), and normal-glucose-to-high-glucose at L3 (NGtoG), with or without 100 µM folic acid (n = 5 to 8 worms per condition).

Intrauterine hatching and egg-laying assays

Synchronised L4 hermaphrodites were transferred to the indicated dietary-treatment plates and scored daily for internally hatched larvae visible through the cuticle at 20× magnification. Bagged hermaphrodites per cohort of 30 were recorded as the cumulative IUH index across the reproductive window. For the acute egg-laying assay, day-1 adults were transferred to M9 buffer containing native *L. paracasei AV47* CFL (Pextract), *L. delbrueckii* CFL (Bextract) or sulfamethoxazole-pretreated *L. paracasei AV47* CFL (SUX), and eggs released into the buffer were counted at 5, 10 and 60 min per cohort of 10 animals (n = 10 cohorts per condition). Comparisons used unpaired Welch t-tests.

Residual medium glucose and Sudan III lipid staining

For residual glucose, day-3 adults reared in 2% glucose were transferred to defined OCM treatments (vehicle control; SAM 50 µM; SAH 50 µM; methotrexate 1 µM; UMFA 100 µM; SAM plus UMFA; and methotrexate plus SAM), and after 72 h the residual media were assayed for residual glucose by glucose-oxidase/peroxidase colorimetry with absorbance read at 505 nm (replicates = 7 per group). 20 worms/µL, enumerated by Scanlan et al. (49) method, was used in the medium containing glucose OCM treatments and bacterial treatments. For Sudan III staining, day-3 adults were fixed in 1% paraformaldehyde, permeabilised by three freeze-thaw cycles, stained with saturated Sudan III in 70%

ethanol for 30 min at 25°C, washed and imaged in colour. The Sudan III staining is reported as a qualitative observation only.

Hydrogen peroxide survival

Day-1 adults (n = 18 wells of 10 animals per condition across three replicate plates) were transferred to flat-bottom 96-well plates containing M9 buffer with 2 mM hydrogen peroxide and scored every 60 min for 6 h. Animals failing to respond to a platinum-pick touch were scored as dead. Two-way ANOVA on percentage survival, with strain and time as fixed effects, was followed by Tukey HSD post-hoc.

Body bending assay

Day-1 adults were transferred from the diet plate to a 50 µL drop of M9 buffer on an unseeded NGM plate. After a 30 s acclimatisation, complete sinusoidal body bends were counted manually for 1 min per animal by an observer blinded to condition (n = 20 animals per condition, three independent biological replicates). One-way ANOVA with Tukey HSD was used for comparisons.

Statistics

All experiments were performed with at least three biological replicates on independent days. Continuous data were tested for normality (Shapiro-Wilk) and equality of variance (Levene). Parametric tests (ANOVA with Tukey HSD) were used where assumptions were satisfied, and non-parametric alternatives (Kruskal-Wallis with Dunn post-hoc and Benjamini-Hochberg correction; Wilcoxon rank-sum with Bonferroni adjustment) where they were not. All analyses were performed in R 4.3 (50) and ImageJ (Fiji distribution) was used for image quantification.

Declarations

Funding

No funding was received to assist with the preparation of this manuscript. laboratory facilities, equipment and consumables were provided in kind by the P.G. Department of Biosciences, Sardar Patel University.

Competing interests

The authors have no relevant financial or non-financial interests to disclose.

Ethics approval

The study was approved by the Institutional Ethics Committee of Bhaikaka University (approval number IEC/BU/2025/Ex.49/184/2025). The salivary *Lacticaseibacillus paracasei* strain AV47 was recovered from a healthy, non-diabetic adult donor under this approval, and all procedures involving the human-

derived isolate were performed in accordance with the principles of the Declaration of Helsinki and relevant institutional and national guidelines. *Caenorhabditis elegans* is an invertebrate; its use does not require animal-research ethics approval.

Consent to participate

Informed consent was obtained from the individual donor from whom the salivary bacterial isolate (*L. paracasei* AV47) was recovered.

Consent to publish

Not applicable. The manuscript contains no data, images or videos from which an individual person can be identified.

Data availability

The partial 16S rRNA gene sequence of *L. paracasei* strain AV47 (1,336 bp) has been deposited in NCBI GenBank under accession number PZ458082.The datasets generated and analysed during the current study are provided in the Zenodo repository, DOI 10.5281/zenodo.20569608 and any extra images or microscopy videos are available from the corresponding authors on reasonable request.

Author contributions

PO, VT and AR conceived and designed the study. PO performed the *C. elegans* experiments, calcium imaging, neurite morphometry, behavioural and biochemical assays, and analysed the data. AR, RF, HJ and PC contributed to bacterial culture, cell-free lysate preparation, microbiological vitamin assays and data collection. AR, PB, RM and SN contributed to the isolation and characterisation of the *Lacticaseibacillus paracasei* strain AV47 and to clinical interpretation of the findings. PO wrote the first draft of the manuscript, and VT supervised the work and critically revised it. All authors read and approved the final manuscript.

Clinical trial number

Not applicable.

References

1. Pfeiffer CM, Sternberg MR, Fazili Z, Yetley EA, Lacher DA, Bailey RL, Johnson CL (2015) Unmetabolized folic acid is detected in nearly all serum samples from US children, adolescents, and adults. J Nutr 145(3):520–531. https://doi.org/10.3945/jn.114.201210

2. Xiong H, Li X, Cheng S, Chen P, Guo S, Huang X, Lu Y (2022) Folate status and mortality in US adults with diabetes: a nationally representative cohort study. Front Cardiovasc Med 9:802247. https://doi.org/10.3389/fcvm.2022.802247
3. Wang D, Zhai JX, Liu DW (2017) Serum folate, vitamin B12 levels and diabetic peripheral neuropathy in type 2 diabetes: a meta-analysis. Mol Cell Endocrinol 443:72–79. https://doi.org/10.1016/j.mce.2017.01.006
4. White JG, Southgate E, Thomson JN, Brenner S (1986) The structure of the nervous system of the nematode Caenorhabditis elegans. Philos Trans R Soc Lond B Biol Sci 314(1165):1–340. https://doi.org/10.1098/rstb.1986.0056
5. Chen TW, Wardill TJ, Sun Y, Pulver SR, Renninger SL, Baohan A, Schreiter ER, Kerr RA, Orger MB, Jayaraman V, Looger LL, Svoboda K, Kim DS (2013) Ultrasensitive fluorescent proteins for imaging neuronal activity. Nature 499(7458):295–300. https://doi.org/10.1038/nature12354
6. Ruiz MA, Dumesnil DR, Shah A, Ladage ML, Song L, Padilla PA (2025) Glucose promotes neuron morphology abnormalities and egg-laying defects dependent on the serotonin signaling pathway in Caenorhabditis elegans. https://doi.org/10.1101/2025.09.20.677429. bioRxiv
7. Annibal A, Tharyan RG, Schonewolff MF, Tam H, Latza C, Auler MMK, Gronke S, Partridge L, Antebi A (2021) Regulation of the one carbon folate cycle as a shared metabolic signature of longevity. Nat Commun 12:3486. https://doi.org/10.1038/s41467-021-23856-9
8. Rahman SS, Bhattacharjee S, Motwani S, Prakash G, Ujjainiya R, Chitkara S, Nair T, Keerthana RS, Sengupta S, Mukhopadhyay A (2025) Methionine cycle in C. elegans serotonergic neurons regulates diet-dependent behaviour and longevity through neuron-gut signaling. Nat Commun 16:5118. https://doi.org/10.1038/s41467-025-60475-0
9. Peesapati RS, Austin-Byler BL, Nawaz FZ, Stevenson JB, Mais SA, Kaya RN, Hassan MG, Khanal N, Wells AC, Ghiai D, Garikapati AK, Selhub J, Kipreos ET (2024) A specific folate activates serotonergic neurons to control C. elegans behavior. Nat Commun 15:8471. https://doi.org/10.1038/s41467-024-52738-z
10. LeBlanc JG, Milani C, de Giori GS, Sesma F, van Sinderen D, Ventura M (2013) Bacteria as vitamin suppliers to their host: a gut microbiota perspective. Curr Opin Biotechnol 24(2):160–168. https://doi.org/10.1016/j.copbio.2012.08.005
11. Balashova OA, Panoutsopoulos AA, Visina O, Selhub J, Knoepfler PS, Borodinsky LN (2024) Noncanonical function of folate through folate receptor 1 during neural tube formation. Nat Commun 15:1642. https://doi.org/10.1038/s41467-024-45775-1
12. Nawaz FZ, Kipreos ET (2022) Emerging roles for folate receptor FOLR1 in signaling and cancer. Trends Endocrinol Metab 33(3):159–174. https://doi.org/10.1016/j.tem.2021.12.003
13. Wibowo AS, Singh M, Reeder KM, Carter JJ, Kovach AR, Meng W, Ratnam M, Zhang F, Dann CE (2013) Structures of human folate receptors reveal biological trafficking states and diversity in folate and antifolate recognition. Proc Natl Acad Sci U S A 110(38):15180–15188. https://doi.org/10.1073/pnas.1308827110

14. Salminen S, Collado MC, Endo A, Hill C, Lebeer S, Quigley EMM, Sanders ME, Shamir R, Swann JR, Szajewska H, Vinderola G (2021) The International Scientific Association of Probiotics and Prebiotics (ISAPP) consensus statement on the definition and scope of postbiotics. Nat Rev Gastroenterol Hepatol 18(9):649–667. https://doi.org/10.1038/s41575-021-00440-6
15. Wang S, Ahmadi S, Nagpal R, Jain S, Mishra SP, Kavanagh K, Zhu X, Wang Z, McClain DA, Kritchevsky SB, Kitzman DW, Yadav H (2020) Lipoteichoic acid from the cell wall of a heat-killed Lactobacillus paracasei D3-5 ameliorates aging-related leaky gut, inflammation and improves physical and cognitive functions: from C. elegans to mice. GeroScience 42(1):333–352. https://doi.org/10.1007/s11357-019-00137-4
16. Kishimoto S, Nono M, Makizaki Y, Tanaka Y, Ohno H, Nishida E, Uno M (2024) Lactobacillus paracasei subsp. paracasei 2004 improves health and lifespan in Caenorhabditis elegans. Sci Rep 14:10453. https://doi.org/10.1038/s41598-024-60580-y
17. Kumaree KK, Prasanth MI, Sivamaruthi BS, Kesika P, Tencomnao T, Chaiyasut C, Prasansuklab A (2023) Lactobacillus paracasei HII01 enhances lifespan and promotes neuroprotection in Caenorhabditis elegans. Sci Rep 13:16707. https://doi.org/10.1038/s41598-023-43846-9
18. Capozzi V, Russo P, Duenas MT, Lopez P, Spano G (2012) Lactic acid bacteria producing B-group vitamins: a great potential for functional cereals products. Appl Microbiol Biotechnol 96(6):1383–1394. https://doi.org/10.1007/s00253-012-4440-2
19. Magnusdottir S, Ravcheev D, de Crecy-Lagard V, Thiele I (2015) Systematic genome assessment of B-vitamin biosynthesis suggests co-operation among gut microbes. Front Genet 6:148. https://doi.org/10.3389/fgene.2015.00148
20. Brenner S (1974) The genetics of Caenorhabditis elegans. Genetics 77(1):71–94. https://doi.org/10.1093/genetics/77.1.71
21. Laino JE, LeBlanc JG, Savoy de Giori G (2012) Production of natural folates by lactic acid bacteria starter cultures isolated from artisanal Argentinean yogurts. Can J Microbiol 58(5):581–588. https://doi.org/10.1139/w2012-026
22. De Guzman ACV, Kang S, Kim EJ, Kim JH, Jang N, Cho JH, Choi SS (2022) High-glucose diet attenuates the dopaminergic neuronal function in C. elegans, leading to the acceleration of the aging process. ACS Omega 7(36):32339–32348. https://doi.org/10.1021/acsomega.2c03384
23. Schlotterer A, Kukudov G, Bozorgmehr F, Hutter H, Du X, Oikonomou D, Ibrahim Y, Pfisterer F, Rabbani N, Thornalley P, Sayed A, Fleming T, Humpert P, Schwenger V, Zeier M, Hamann A, Stern D, Brownlee M, Bierhaus A, Nawroth P, Morcos M (2009) C. elegans as model for the study of high glucose-mediated life-span reduction. Diabetes 58(11):2450–2456. https://doi.org/10.2337/db09-0567
24. Adler CE, Fetter RD, Bargmann CI (2006) UNC-6/Netrin induces neuronal asymmetry and defines the site of axon formation. Nat Neurosci 9(4):511–518. https://doi.org/10.1038/nn1666
25. Yim J, Kim G, Lee BW, Kang ES, Cha BS, Kim JH, Cho JW, Lee SG, Lee YH (2018) Relationship between circulating netrin-1 concentration, impaired fasting glucose, and newly diagnosed type 2 diabetes. Front Endocrinol (Lausanne) 9:691. https://doi.org/10.3389/fendo.2018.00691

26. Collins KM, Bode A, Fernandez RW, Tanis JE, Brewer JC, Creamer MS, Koelle MR (2016) Activity of the C. elegans egg-laying behavior circuit is controlled by competing activation and feedback inhibition. eLife 5:e21126. https://doi.org/10.7554/eLife.21126
27. Schafer WR (2005) Egg-laying. WormBook 1–7. https://doi.org/10.1895/wormbook.1.38.1
28. Trent C, Tsung N, Horvitz HR (1983) Egg-laying defective mutants of the nematode Caenorhabditis elegans. Genetics 104(4):619–647. https://doi.org/10.1093/genetics/104.4.619
29. Noble T, Stieglitz J, Srinivasan S (2013) An integrated serotonin and octopamine neuronal circuit directs the release of an endocrine signal to control C. elegans body fat. Cell Metab 18(5):672–684. https://doi.org/10.1016/j.cmet.2013.09.007
30. Srinivasan S, Sadegh L, Elle IC, Christensen AGL, Faergeman NJ, Ashrafi K (2008) Serotonin regulates C. elegans fat and feeding through independent molecular mechanisms. Cell Metab 7(6):533–544. https://doi.org/10.1016/j.cmet.2008.04.012
31. Sze JY, Victor M, Loer C, Shi Y, Ruvkun G (2000) Food and metabolic signalling defects in a Caenorhabditis elegans serotonin-synthesis mutant. Nature 403(6769):560–564. https://doi.org/10.1038/35000609
32. Burkewitz K, Zhang Y, Mair WB (2014) AMPK at the nexus of energetics and aging. Cell Metab 20(1):10–25. https://doi.org/10.1016/j.cmet.2014.03.002
33. Mair W, Morantte I, Rodrigues APC, Manning G, Montminy M, Shaw RJ, Dillin A (2011) Lifespan extension induced by AMPK and calcineurin is mediated by CRTC-1 and CREB. Nature 470(7334):404–408. https://doi.org/10.1038/nature09706
34. Ogawa T, Tsubakiyama R, Kanai M, Koyama T, Fujii T, Iefuji H, Soga T, Kume K, Miyakawa T, Hirata D, Mizunuma M (2016) Stimulating S-adenosyl-L-methionine synthesis extends lifespan via activation of AMPK. Proc Natl Acad Sci U S A 113(42):11913–11918. https://doi.org/10.1073/pnas.1604047113
35. Sawin ER, Ranganathan R, Horvitz HR (2000) C. elegans locomotory rate is modulated by the environment through a dopaminergic pathway and by experience through a serotonergic pathway. Neuron 26(3):619–631. https://doi.org/10.1016/s0896-6273(00)81199-x
36. Lee SJ, Murphy CT, Kenyon C (2009) Glucose shortens the life span of C. elegans by downregulating DAF-16/FOXO activity and aquaporin gene expression. Cell Metab 10(5):379–391. https://doi.org/10.1016/j.cmet.2009.10.003
37. Brownlee M (2001) Biochemistry and molecular cell biology of diabetic complications. Nature 414(6865):813–820. https://doi.org/10.1038/414813a
38. Nishikawa T, Edelstein D, Du XL, Yamagishi S, Matsumura T, Kaneda Y, Yorek MA, Beebe D, Oates PJ, Hammes HP, Giardino I, Brownlee M (2000) Normalizing mitochondrial superoxide production blocks three pathways of hyperglycaemic damage. Nature 404(6779):787–790. https://doi.org/10.1038/35008121
39. Banerjee RV, Matthews RG (1990) Cobalamin-dependent methionine synthase. FASEB J 4(5):1450–1459. https://doi.org/10.1096/fasebj.4.5.2407589

40. Yajnik CS, Deshpande SS, Jackson AA, Refsum H, Rao S, Fisher DJ, Bhat DS, Naik SS, Coyaji KJ, Joglekar CV, Joshi N, Lubree HG, Deshpande VU, Rege SS, Fall CHD (2008) Vitamin B12 and folate concentrations during pregnancy and insulin resistance in the offspring: the Pune Maternal Nutrition Study. Diabetologia 51(1):29–38. https://doi.org/10.1007/s00125-007-0793-y
41. Blackwell TK, Steinbaugh MJ, Hourihan JM, Ewald CY, Isik M (2015) SKN-1/Nrf, stress responses, and aging in Caenorhabditis elegans. Free Radic Biol Med 88(Pt B) 290–301. https://doi.org/10.1016/j.freeradbiomed.2015.06.008
42. Stipanuk MH (2004) Sulfur amino acid metabolism: pathways for production and removal of homocysteine and cysteine. Annu Rev Nutr 24:539–577. https://doi.org/10.1146/annurev.nutr.24.012003.132418
43. Mosharov E, Cranford MR, Banerjee R (2000) The quantitatively important relationship between homocysteine metabolism and glutathione synthesis by the transsulfuration pathway and its regulation by redox changes. Biochemistry 39(42):13005–13011. https://doi.org/10.1021/bi001088w
44. Jankovic-Karasoulos T, Smith MD, Leemaqz S, Mittinty M, Williamson J, McCullough D, Arthurs AL, Dekker GA, Roberts CT (2025) Maternal folate excess, placental hormones, and gestational diabetes mellitus. Nutrients 17(17):2863. https://doi.org/10.3390/nu17172863
45. Stiernagle T (2006) Maintenance of C. elegans. WormBook 1–11. https://doi.org/10.1895/wormbook.1.101.1
46. Porta-de-la-Riva M, Fontrodona L, Villanueva A, Ceron J (2012) Basic Caenorhabditis elegans methods: synchronization and observation. J Vis Exp 64:e4019. https://doi.org/10.3791/4019
47. Polansky M (1981) Microbiological assay of vitamin B-6 in foods. In: Leklem JE, Reynolds RD (eds) Methods in vitamin B-6 nutrition: analysis and status assessment. Plenum, New York, pp 21–44
48. Tsuda H, Matsumoto T, Ishimi Y (2012) Time reduction of vitamin B6 and inositol assay by using lyophilized Saccharomyces cerevisiae ATCC 9080. J Nutr Sci Vitaminol (Tokyo) 58(2):149–151. https://doi.org/10.3177/jnsv.58.149
49. Scanlan LD, Lund SP, Coskun SH, Hanna SK, Johnson ME, Sims CM, Brignoni K, Lapasset P, Petersen EJ, Elliott JT, Nelson BC (2018) Counting Caenorhabditis elegans: protocol optimization and applications for population growth and toxicity studies in liquid medium. Sci Rep 8(1):904. https://doi.org/10.1038/s41598-018-19187-3
50. R Core Team (2023) R: a language and environment for statistical computing. R Foundation for Statistical Computing, Vienna, Austria. https://www.R-project.org/

Figures



Figure 1

Identification of 10-formyl-THF as the possible neuroprotective effector of L. paracasei AV47 postbiotic and its competitive abolition by unmetabolized folic acid under hyperglycaemia. (A)*Experimental schematic showing difference in fluorescence post stimulus as seen under the microscope Scale bar (blue line) = 10 µm. C. elegans expressing GCaMP7 in NSM serotonergic neurons were maintained on five dietary conditions (E. coli OP50, L. delbrueckii, L. paracasei AV47, L. paracasei AV47 CFL postbiotic) with or without*

2% dietary glucose and/or UMFA supplementation. ***(B)****Quantitative vitamin profiling of bacterial supernatants. L. paracasei AV47 produces methylcobalamin at 100 µg/L versus 4 µg/L in L. delbrueckii (25-fold), vitamin B6 at 1,523 versus 100 µg/L (15.7-fold), and total folate at 1,241 versus 133 µg/L (9.3-fold).* ***(C, D)*** *Averaged representative GCaMP traces of NSM calcium transients across dietary conditions (C, live bacterial cells; D, Cell free lysate), showing near-complete suppression of evoked transient amplitude under chronic glucose and full rescue by L. paracasei AV47 and its CFL but not by L. delbrueckii.* ***(E)*** *Bar graph (mean ± SEM) of response magnitude ($\Delta F/F_0$, post-minus-pre stimulus) for the initial extract validation dataset. Compact letter display (CLD) above bars denotes Tukey HSD groupings ($p < 0.05$). L. paracasei AV47 in glucose is significantly rescued relative to L. delbrueckii glucose + UMFA ($p = 3.0 \times 10^{-4}$); co-addition of UMFA to L. paracasei AV47 + glucose abolishes rescue, converging with the L. delbrueckii glucose + UMFA condition ($p = 1.0$).* ***(F)*** *Component-breakdown dataset. Pure 10-formyl-THF phenocopies L. paracasei AV47 CFL under glucose ($p = 0.64$). Heat-aged CFL (thermolabile active species; Pea_g vs. FTHF_g, $p = 2.7 \times 10^{-4}$) and sulfonamide-pretreated CFL (downstream of DHPS; Pes_g vs. FTHF_g, $p = 1.1 \times 10^{-6}$) both lose rescue capacity. Addition of UMFA under glucose abolishes rescue by both L. paracasei AV47 CFL ($p = 1.6 \times 10^{-9}$) and pure 10-f-THF ($p = 3.1 \times 10^{-3}$), consistent with competitive displacement of 10-f-THF at FOLR-1/GON-2. All statistical comparisons by one-way ANOVA with Tukey HSD correction*

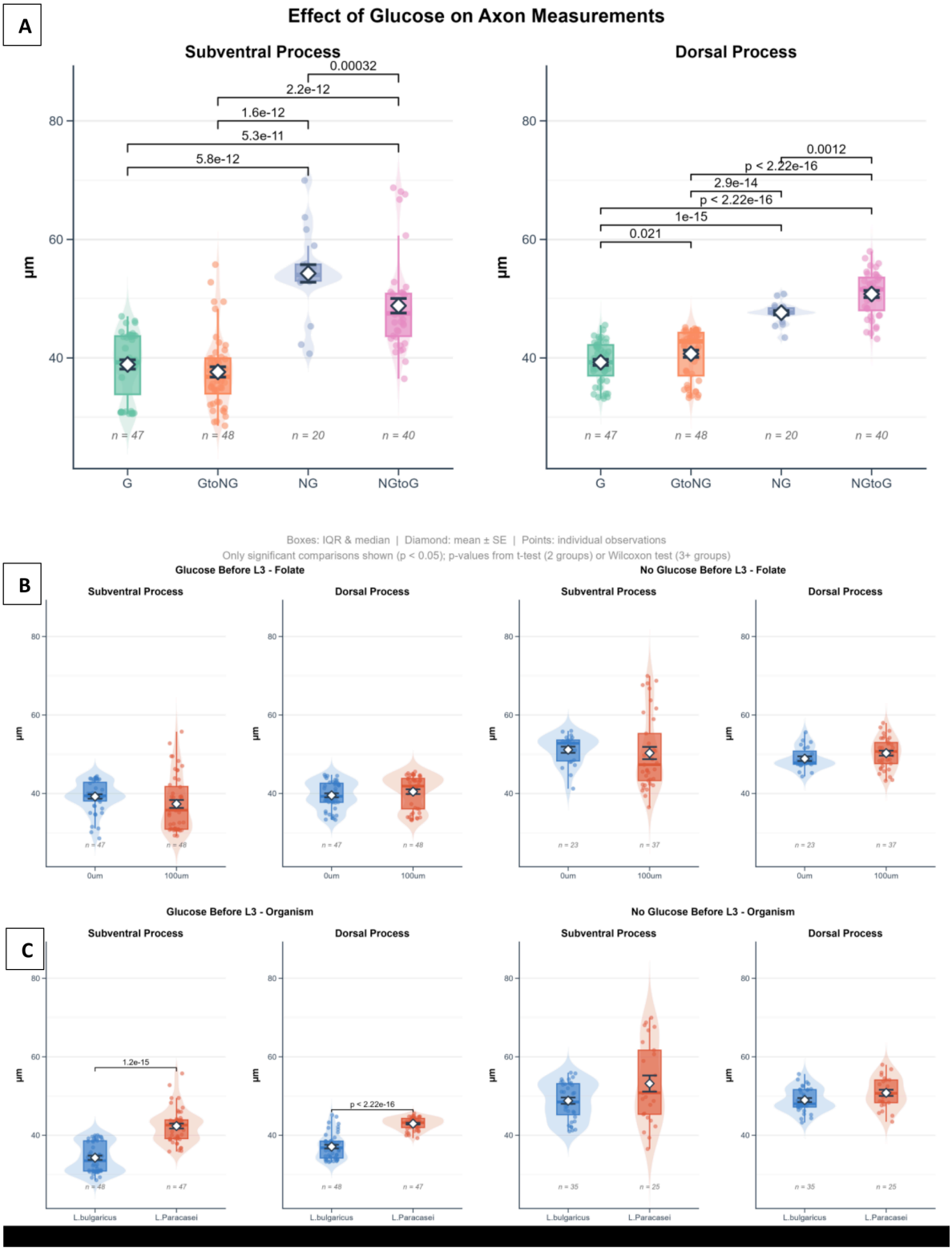


Figure 2

NSM axon length shortening effect of glucose is age dependent and negated by L. paracasei AV47. (A) Axon length measurements for subventral and dorsal processes under different glucose conditions. Animals were maintained in constant excess glucose (G) or normal glucose (NG), or subjected to dietary transitions (GtoNG and NGtoG) at the end of the L3 stage. (B) Folate and (C) bacterial feeding conditions, each stratified by pre-L3 glucose history (Glucose Before L3 and No Glucose Before L3). Animals were

exposed to either 0 μM or 100 μM folate, or fed L. delbrueckii or L. paracasei AV47. NSM subventral and dorsal process lengths were measured in day-3 adults across four glucose regimes: continuous excess glucose from L1 (G), normal glucose (NG), excess glucose to normal glucose at L3 (GtoNG), and normal glucose to excess glucose at L3 (NGtoG). Violin and box plots show full distributions, with diamonds indicating means ± SE and boxes showing the interquartile range and median; points are individual animals. Only significant comparisons are shown ($p < 0.05$; p-values from t-test for two-group and Wilcoxon test for four-group comparisons). L. paracasei AV47 is associated with preservation of both processes under developmental glucose exposure, and the pre-L3 glucose effect (G, GtoNG) is not restored by adult withdrawal.

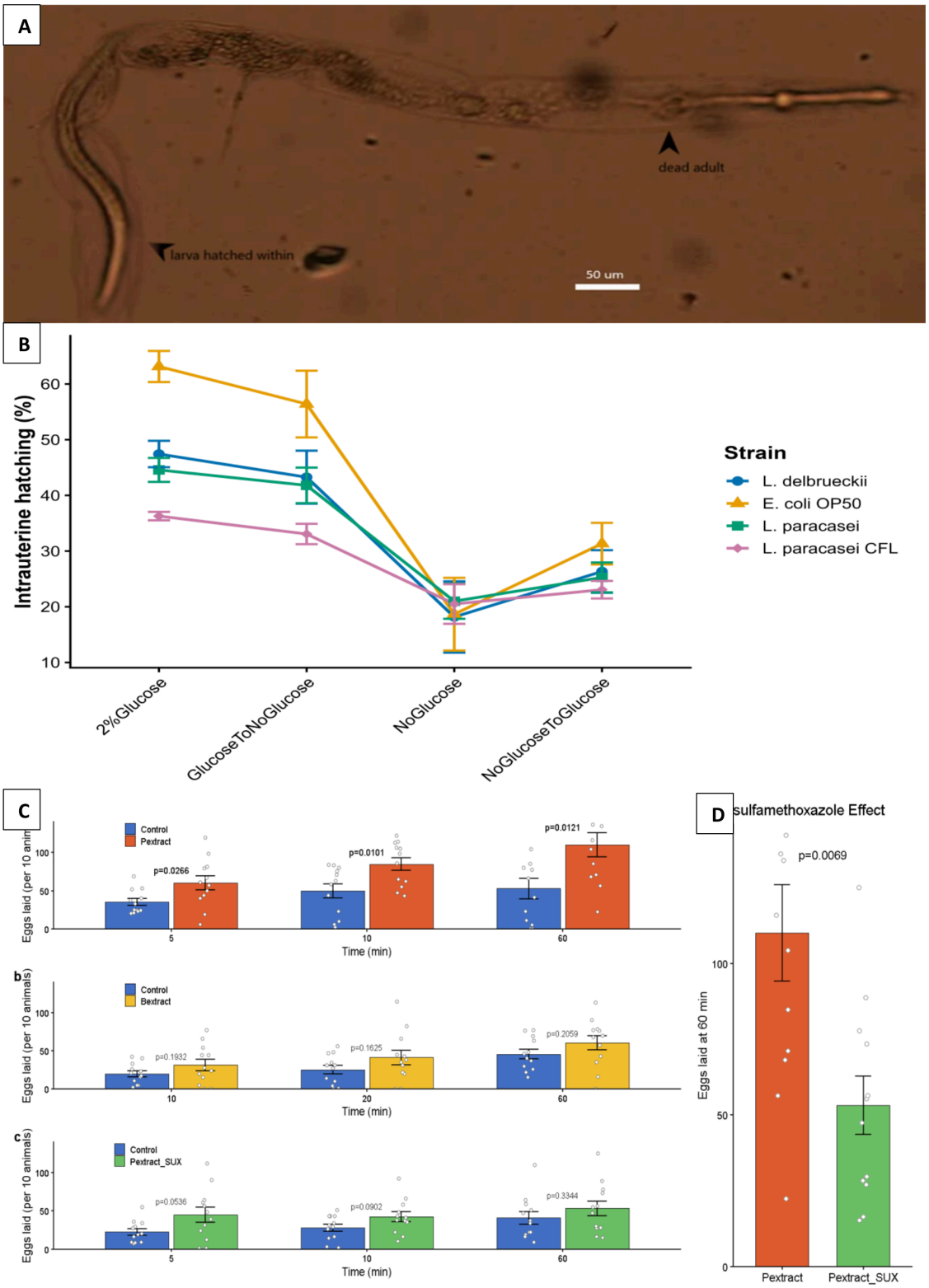


Figure 3

L. paracasei AV47 CFL reduces intrauterine hatching and acutely stimulates HSN-driven egg-laying. *(A) Representative micrograph of a bagged hermaphrodite with an internally hatched L1 larva visible through the cuticle. Scale bar 50 um. (B) IUH burden per cohort of 30 hermaphrodites across diet and glucose regimes: chronic 2 percent glucose (GlucoseControl), glucose-to-no-glucose at L3 (GlucoseToNoGlucose), no-glucose (NoGlucose) and no-glucose-to-glucose at L3 (NoGlucoseToGlucose). Lines show mean and SD;*

n = 7 cohorts of 30 hermaphrodites per condition. Glucose is the dominant driver of IUH; live L. paracasei AV47 and L. paracasei AV47 CFL both attenuate the effect, with CFL producing the largest reduction (approximately 43 percent relative to OP50). (C) Eggs released into buffer per 10 animals at 5, 10 and 60 min following acute exposure to L. paracasei AV47 CFL (Pextract, top), L. delbrueckii CFL (Bextract, middle), or sulfamethoxazole-pretreated L. paracasei AV47 CFL (SUX, bottom). Pextract is associated with a significant increase in egg-laying at all three time points (5 min p = 0.027; 10 min p = 0.010; 60 min p = 0.012; Welch t-test). Bextract is not associated with a significant change. SUX pretreatment eliminates the Pextract activity. Bars are mean and SEM, n = 10 cohorts per time point. (D) Side-by-side comparison of egg laying after 60 min of L. paracasei AV47 Pextract exposure in the presence or absence of sulfamethoxazole pretreatment, showing a significant reduction in the Pextract-induced increase in egg laying following sulfamethoxazole exposure (Welch's t-test, p = 0.0069)

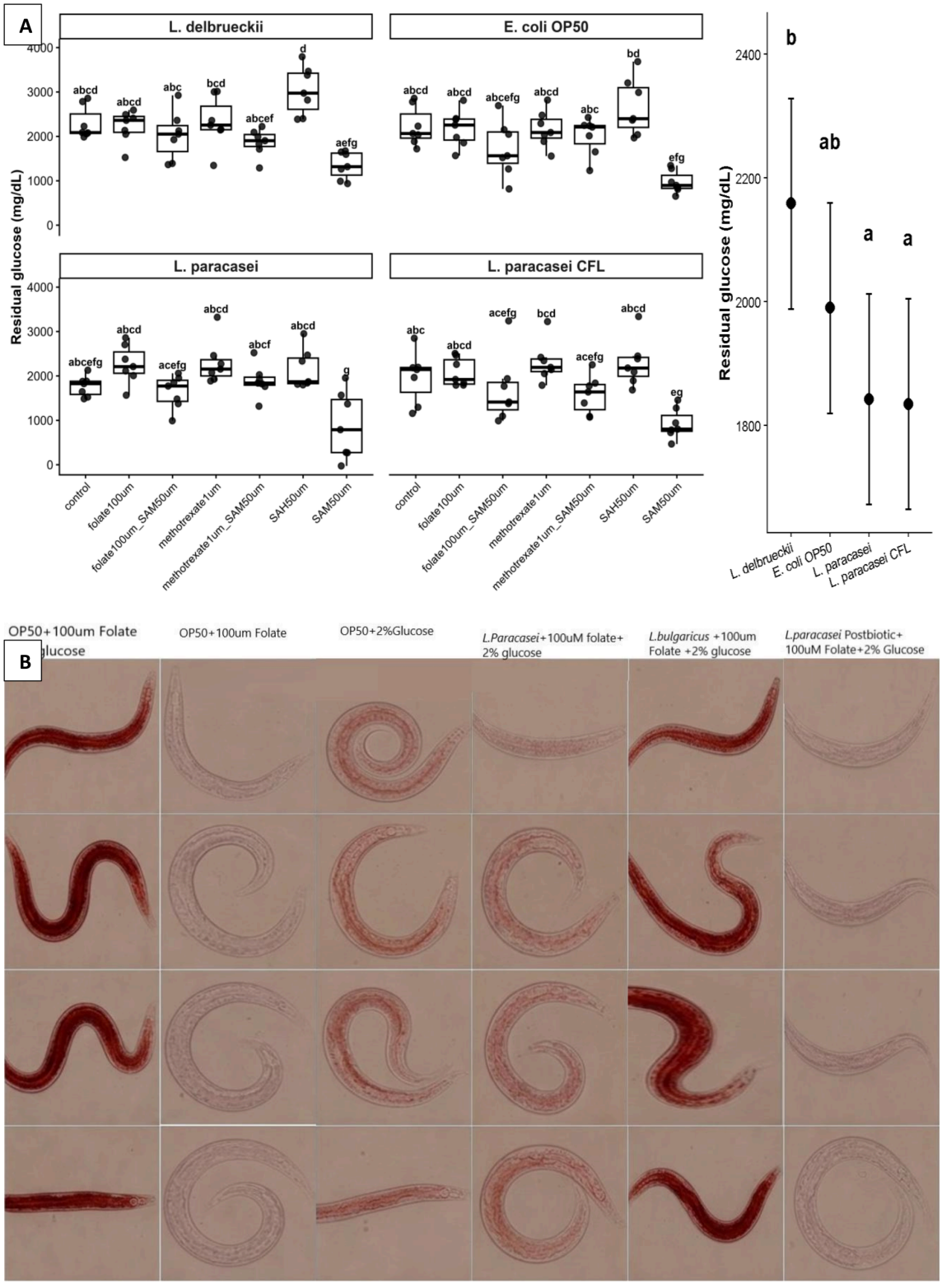


Figure 4

L. paracasei AV47 CFL is associated with lower residual medium glucose and with qualitatively reduced intestinal lipid staining.*(A) Residual culture-medium glucose (mg/dL) across four bacterial conditions (OP50, live L. paracasei AV47, L. paracasei AV47 CFL, L. delbrueckii) under seven OCM perturbations: vehicle control; SAM 50 uM; SAH 50 uM; methotrexate (MTX) 1 uM; 100 uM UMFA; MTX plus SAM; and UMFA plus SAM. SAM lowers residual glucose by approximately 40 to 55 percent under every diet; SAH*

elevates residual glucose under L. delbrueckii but not under L. paracasei AV47 or its CFL. n = 7 replicates per group; significance marks Tukey HSD pairwise contrasts (mean and SD shown). (B) Representative Sudan III-stained day-3 adults across six dietary conditions: OP50, OP50 plus 100 uM folate, OP50 plus 2 percent glucose, L. paracasei AV47 plus 100 uM folate plus 2 percent glucose, L. delbrueckii plus 100 uM folate plus 2 percent glucose, and L. paracasei AV47 CFL plus 100 uM folate plus 2 percent glucose. OP50- and L. delbrueckii-treated worms show broad intestinal red staining; the L. paracasei AV47 CFL condition shows visibly less intense staining. The Sudan III data are presented as a qualitative observation only; n = 4 cohorts per condition was underpowered for quantitative inferential analysis, and a bar-graph quantification is therefore not reported

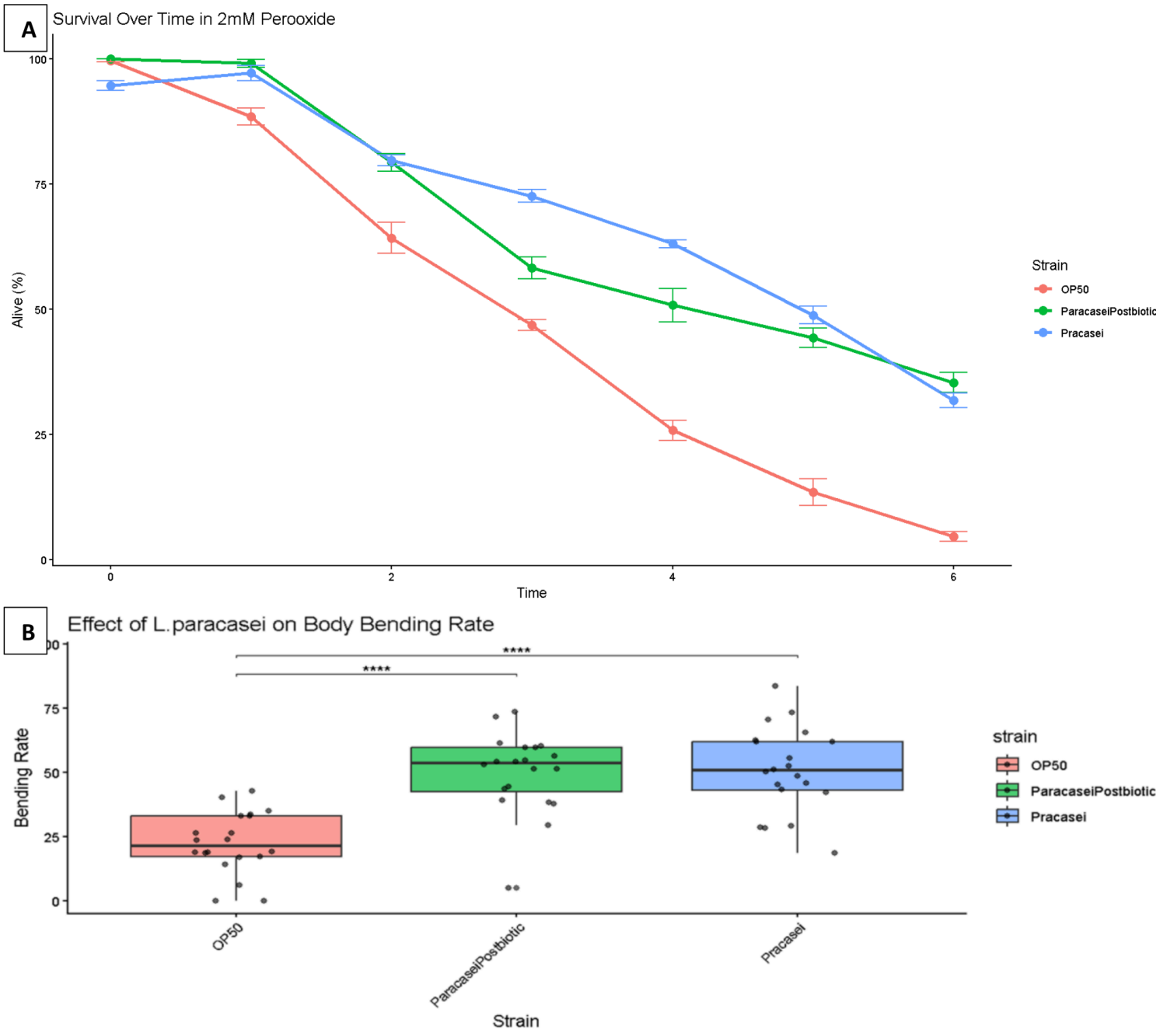


Figure 5

A. L. paracasei AV47 live and L. paracasei AV47 CFL are associated with an approximately 7-fold survival advantage under 2 mM hydrogen peroxide. *Percentage survival across time (hours) for day-1 adults exposed to 2 mM H2O2 in M9 buffer, scored every 60 min for 6 h; n = 18 wells of 10 animals per condition (three replicate plates). Two-way ANOVA returned highly significant main effects of strain (F(2, 105) = 281.87, p less than 0.001, partial eta-squared = 0.84), of time (F(6, 105) = 795.76, p less than 0.001, partial eta-squared = 0.98), and a significant strain by time interaction (F(12, 105) = 22.73, p less than 0.001, partial eta-squared = 0.72). Live L. paracasei AV47 and L. paracasei AV47 CFL both retain approximately 32 to 35 percent survival at 6 h, compared to 4.5 percent on OP50. Live and CFL preparations did not differ at 5 and 6 h (p = 0.169 and 0.330 respectively). Error bars show standard deviation.* ***(B).*** *L. paracasei AV47 live and L. paracasei AV47 CFL are associated with approximately double the spontaneous body-bending rate of OP50. Body-bending rate (complete sinusoidal bends per minute in M9 buffer) for day-1 adults reared on OP50, L. paracasei AV47 CFL, and live L. paracasei AV47. n = 20 animals per condition across three independent biological replicates, scored by an observer blinded to condition; one-way ANOVA F(2, 57) = 23.91, p less than 0.001, eta-squared = 0.46. Both L. paracasei AV47 conditions produce approximately 50 bends/min versus approximately 22 bends/min on OP50 (delta approximately +28 bends/min, p less than 0.001). Live and CFL preparations did not differ (delta = 0.95, p = 0.978). The four asterisks denote p less than 0.0001 (Tukey HSD)*

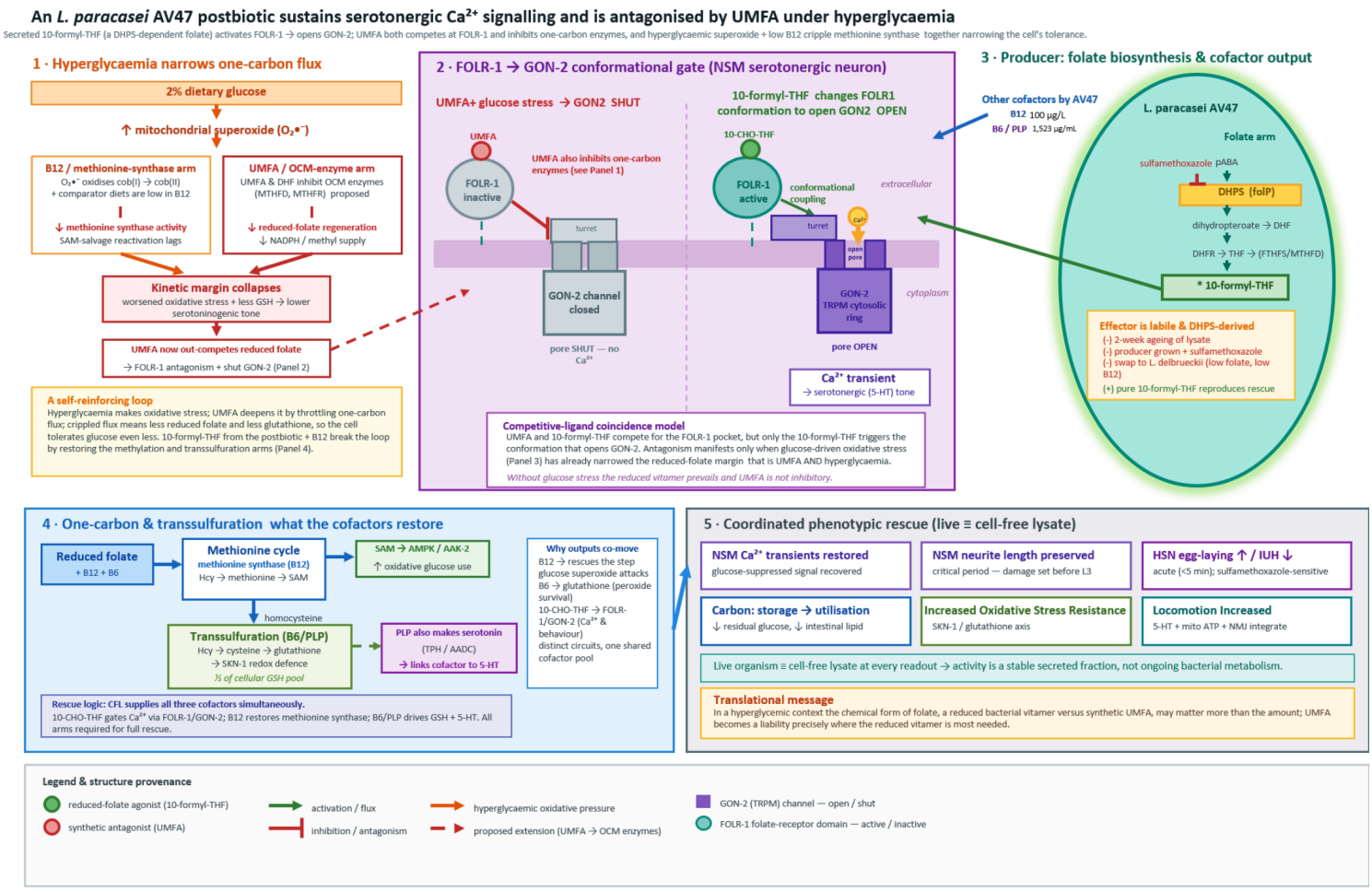


Figure 6

AV47-derived 10-formyl-THF, vitamin B12, and vitamin B6 rescue hyperglycemia-induced impairment of serotonergic signaling and one-carbon metabolism; this rescue is abolished by UMFA